Nanotechnology **20** (2009) 125503 (8pp) doi:10.1088/0957-4484/20/12/125503

A nanoelectronic nose: a hybrid nanowire/carbon nanotube sensor array with integrated micromachined hotplates for sensitive gas discrimination

Po-Chiang Chen, Fumiaki N Ishikawa, Hsiao-Kang Chang, Koungmin Ryu and Chongwu Zhou

Ming-Hsieh Department of Electrical Engineering, University of Southern California, Los Angeles, CA 90089, USA

E-mail: chongwuz@usc.edu

Received 20 December 2008, in final form 30 January 2009
Published 3 March 2009
Online at stacks.iop.org/Nano/20/125503

Abstract

A novel hybrid chemical sensor array composed of individual In_2O_3 nanowires, SnO_2 nanowires, ZnO nanowires, and single-walled carbon nanotubes with integrated micromachined hotplates for sensitive gas discrimination was demonstrated. Key features of our approach include the integration of nanowire and carbon nanotube sensors, precise control of the sensor temperature using the micromachined hotplates, and the use of principal component analysis for pattern recognition. This sensor array was exposed to important industrial gases such as hydrogen, ethanol and nitrogen dioxide at different concentrations and sensing temperatures, and an excellent selectivity was obtained to build up an interesting 'smell-print' library of these gases. Principal component analysis of the sensing results showed great discrimination of those three tested chemicals, and in-depth analysis revealed clear improvement of selectivity by the integration of carbon nanotube sensors. This nanoelectronic nose approach has great potential for detecting and discriminating between a wide variety of gases, including explosive ones and nerve agents.

(Some figures in this article are in colour only in the electronic version)

1. Introduction

Chemical sensing based on a wide variety of nanostructures has attracted great interest in the past few years because of their remarkable properties such as high sensitivity, low cost, and easy fabrication when used as chemical sensors [1–17]. For instance, semiconducting single-walled carbon nanotube (SWNT) field effect transistors (FETs) can be used to detect critical industrial gases, NO_2 and NH_3 [3]. Using SnO_2 nanobelt FETs, detection of dimethyl methylphosphonate (DMMP), which is a nerve agent simulant, can be down to 78 ppb [4]. In our previous work, we also presented highly sensitive In_2O_3 nanowire sensors for which the detection limit of NO_2 was in the ppb level [5]. To improve the device sensitivity, chemical coating treatments [7–9] or nanoparticle decoration [6, 10–13] are widely used. For example, the sensitivity was improved by using Pd-coated SnO_2 nanowire chemoresistors [14], and surface-functionalized flexible silicon nanowire FETs [15] have been used to detect organic vapors at room temperature.

Recently, several research groups have worked on establishing selective chemical sensing for thin film/nanostructure sensors. For instance, the principal component analysis (PCA) was recently applied to nanotube-based chemical sensors and then extended also to nanowire sensors [9]. The KAMINA technology [18], which is based on using a temperature gradient in a sensor array, has also been used for both thin films and nanostructures [19, 20]. This method, however, requires rather high power consumption (∼1 W) [21] and lacks precise control over the temperature for individual sensors.

In this paper, we report a brand-new platform, which can serve as an 'electronic nose' with good 'discrimination

factors', built with four different semiconducting nanostructured materials including In_2O_3 nanowires, SnO_2 nanowires, ZnO nanowires, and SWNTs. Those metal oxide nanowires and SWNTs have significant difference in sensing mechanism. In_2O_3, SnO_2, and ZnO nanowires are n-type semiconductors, which SWNTs are usually p-type semiconductors. Furthermore, those metal oxide nanowires and nanotubes are believed to have different redox response upon exposure to chemicals. This integration of both semiconducting metal oxide nanowire and semiconducting SWNT sensors therefore provides an important discrimination factor for improved selectivity. Furthermore, the integrated micromachined hot plate enables us to control temperature individually and accurately for each sensor, with additional advantages such as ultralow power consumption (∼60 mW) and short response time (20–300 °C within 1 min) [22]. This temperature control works as the second discrimination factor. With these two discrimination factors, we achieved a 'smell-print' library by detecting important industrial gases such as hydrogen, ethanol and nitrogen dioxide. Furthermore, the analyzed sensing results, with aid from the PCA method, [23–25] demonstrated a clear success in the discrimination in these gases. Our approach shows great potential to become a realistic 'electronic nose' with the advantage of compact size, ultralow power consumption, and easy fabrication.

2. Fabrication and experimental details

The hybrid nanostructure sensor array with integrated hot plates began with the fabrication of SiN membranes. The detail of fabrication of SiN membranes can be found in literatures [22]. In brief, we deposited 100 nm SiN on both sides of Si wafers using a low temperature CVD. After that, a photolithography process was carried out to pattern SiN membranes, followed by CF_4 plasma to etch unwanted SiN membranes and 10 wt% KOH to remove Si substrate underneath SiN membranes. We can obtained uniform SiN membranes with a thickness of 100 nm. To achieve diversity in the gas response, chemical sensors were fabricated with four different single-crystalline nanomaterials including In_2O_3 nanowires, SnO_2 nanowires, ZnO nanowires, and SWNTs, which were obtained using different growth methods described below. The In_2O_3 and SnO_2 nanowires were synthesized using a laser ablation method as described in our previous reports [26, 27]. These nanowires, with diameters of about 20 nm and lengths of 5 μm, exhibited defect-free crystalline structure and good electronic characteristics. Vertical ZnO nanowires grown on a-sapphire with diameters of 50 nm and lengths of 10 μm were obtained via a vapor–solid (VS) growth method following previous reports [28, 29]. SWNTs were synthesized directly on SiN membranes via chemical vapor deposition (CVD) at 900 °C with ferritin serving as catalysts, and a methane/ethylene/hydrogen gas mixture as the carbon feedstock [30]. The metal oxide nanowires were sonicated into isopropanol alcohol (IPA) to form different suspensions and then dispersed on the SiN membrane side of the substrates until a reasonable nanowire density was achieved. Photolithography was applied to pattern both source and drain electrodes for chemical sensors and the heating electrodes of hot plates, followed by 100 nm platinum (Pt) deposition using e-beam evaporation. After device fabrication, high voltage bias was applied to burn the unwanted SWNTs between heating electrodes and sensor electrodes.

Table 1. Sensor array test conditions. (Note: the sensing experiments were carried out at room temperature and 200 °C.)

Test gas	Concentration (ppm)
Hydrogen	500
	1000
	2000
Ethanol	50
	100
	200
NO_2	0.1
	1

3. Results and discussion

3.1. Electronic transport measurements

Figure 1(a) shows the photograph of a finished chemical sensor chip, where two arrays of metal electrodes for contacting dispersed nanowires/nanotubes and a wider zigzag Pt heating electrode can be clearly seen residing on a suspended SiN membrane (the bright green area). A chemical sensor array, composed of four different sensor chips, each with individual In_2O_3 nanowire, SnO_2 nanowire, ZnO nanowire, and a SWNT mat, was examined using a field emission scanning electron microscopy (FESEM) and optical microscopy, and the corresponding images are depicted in figure 1(b). The distance between figure-shaped source and drain electrodes is 3 μm and each integrated chip is 1 cm × 1 cm in size. The electron transport measurements of nanowire and SWNT chemical sensors and the micromachined hot plates were carried out using an Agilent 4156B semiconductor parameter analyzer. The chemical sensing experiments were performed using a home-made chemical sensing setup described in our previous work [5, 31–34]. Briefly, the fabricated sensor chips were mounted on a chip carrier inside a sealed chamber with an electrical feedthrough and gas inlet/outlet. The assembled devices from three different metal oxide nanowires and SWNTs were exposed to nitrogen dioxide, ethanol and hydrogen under different concentrations and at varied temperatures (table 1) accomplished by the micromachined hot plates.

The conductance of the nanowire and SWNT sensors at different temperatures (25 and 200 °C) were examined and the corresponding current–voltage (I–V) curves are shown in figure 2. The curves indicate that all these nanomaterials exhibited low-resistance contacts with the Pt source and drain electrodes. Separate nanowire/nanotube devices were made with gate electrodes to examine the n-type semiconducting characteristics of nanowire sensors and p-type semiconducting characteristics of SWNT sensors. Evident from figure 2(b), the nanosensors became more conductive at high temperature than at room temperature. For example, the electrical conductance

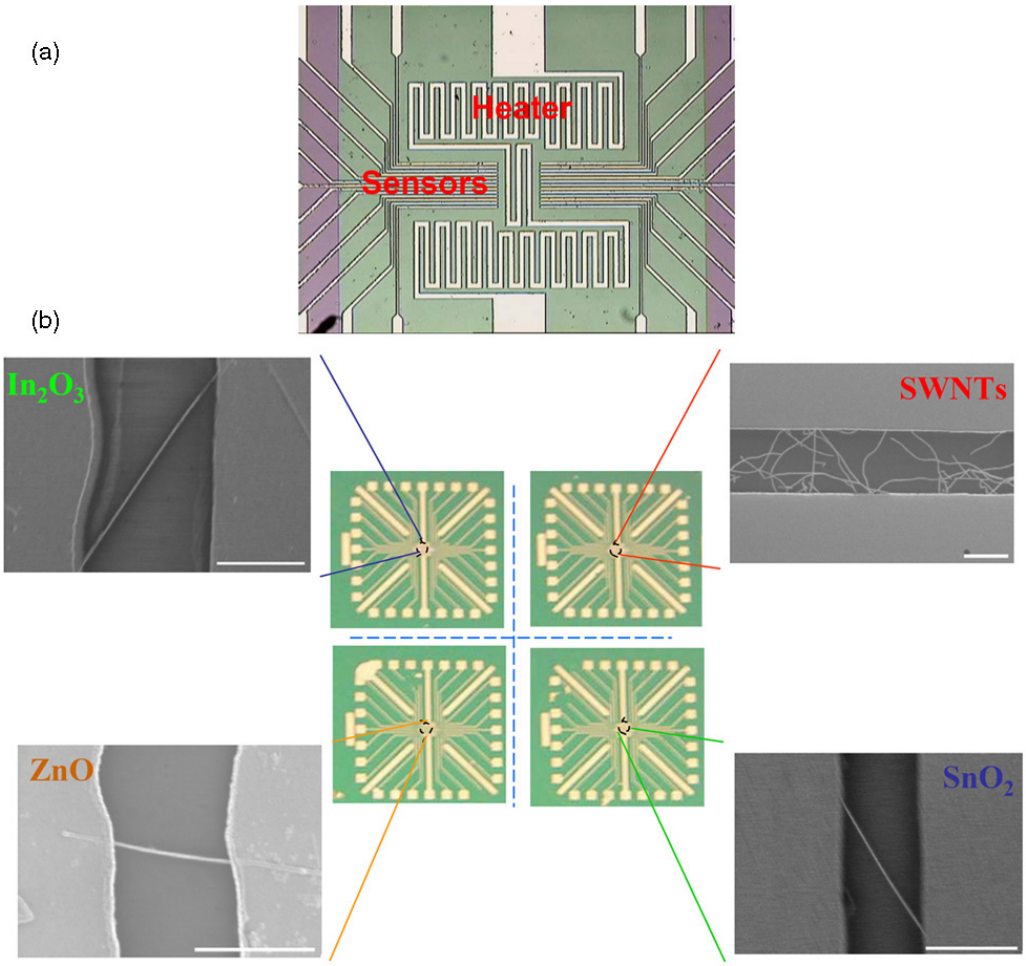

Figure 1. (a) Photograph of a chemical sensor chip with an integrated micromachined hot plate. (b) Hybrid chemical sensor array chip composed of four individual chemical sensors, including individual In_2O_3 nanowire, SnO_2 nanowire, ZnO nanowire, and SWNT chemical sensor chips. The source–drain electrode distance is about 2 μm.

of the In_2O_3 nanowire, SnO_2 nanowire, ZnO nanowire, and a SWNT mat sensor increased from 20 μS, 15 μS, 2 μS, and 5 μS at 25 °C to 23.5 μS, 18.5 μS, 5.5 μS, and 18 μS at 200 °C, respectively. The increase in temperature caused the thermal excitation of carriers and/or the removal of moisture from the nanostructure surface, thus leading to increased carrier concentrations and higher conductance for the semiconducting metal oxide nanowires and SWNTs. In addition, the enhanced reactivity toward surrounding gas molecules at elevated temperatures, and operating the sensors at temperature above 100 °C can eliminate the complicated effect of moisture. In addition, separate nanowire/nanotube devices were made with gate electrodes to confirm the n-type semiconducting characteristics of nanowire sensors and p-type semiconducting characteristics of SWNT sensors.

Regarding the performance of the micromachined hot plates, features like easy temperature tuning and ultralow power consumption were examined. The temperature of the nanosensor hot plate could be easily tuned to any temperature between 25 and 350 °C by applying a voltage bias in the range of 0–10 V. For example, a voltage of 8 V was used to raise the hotplate temperature to 300 °C within 1 min, and then maintained at this temperature with a power consumption of 60 mW [22]. The detail can be found in [22]. This power consumption compares favorably with the ∼1 W consumption of the KAMINA technique [21].

3.2. Chemical sensing experiments

The molecular sensing mechanism for semiconducting nanomaterials mainly relies on the change of electrical conductivity introduced by the surface redox process between nanomaterials and surrounding environment, which can be expressed as [35],

$$\text{RS (relative sensor response)} = \frac{G_1 - G_0}{G_0} \approx \frac{4}{D}\left(\frac{\varepsilon\varepsilon_0}{en_0}\right)^{1/2}(V_{S0}^{1/2} - V_{S1}^{1/2}) \quad (1)$$

where G_1 and G_0 denote the nanowire/nanotube conductance under and before the exposure, respectively. n_0 represent the carrier concentration before exposure to chemicals. D is the diameter of the nanomaterials. ε_0 is the absolute dielectric constant, and ε is the relative dielectric permittivity of the nanostructured materials. V_{S0} is the adsorbate-induced band

bending due to molecules in dry air environment, and V_{S1} is the adsorbate-induced band bending from the exposure of chemicals. The detail can be found in the [36]. To fully understand the different sensing behaviors in different nanomaterials, several theoretical works have been reported to estimate the adsorbate-induced band bending energy and charge transfer to different nanomaterials. For instance, the band bending energy for NH_3 to SnO_2 and (10, 0) carbon nanotube is ∼0.25 eV [37] and ∼0.15 eV [38], respectively, which reveals the different chemical reactions between SnO_2 and carbon nanotubes. Thus, an integration of different nanostructured materials could provide a discrimination factor in our e-nose system.

The as-fabricated hybrid chemical sensors were loaded into a chemical sensing chamber to carry out sensing experiments. Before exposure to chemicals, these devices were first exposed to 254 nm deep UV light in vacuum for 10 min to remove adsorbed moisture and oxygen molecules, and then dry air was fed into the chamber as background gas to simulate practical sensing environment. The sensing experiments were carried out to expose the sensors to three consecutive gas pluses with different concentrations and chemicals (shown in table 1). The sensing behaviors are highly reproducible and the experimental error bars are less than 1%. Figure 3 shows the sensing experiment data after normalization.

As is well known, hydrogen and ethanol are not easy to be detected at room temperature using solid-state sensors. Armed with the integrated hot plates, we successfully detected hydrogen and ethanol in ambient environment with only localized heating to the nanowire/nanotube sensor. Figure 3(a) plots the isothermal response of the current flowing in metal oxide nanowire and SWNT sensors as a function of time under 500 ppm hydrogen diluted in air at 200 °C. As one can see, the electrical current increased by 12.4%, 17.7%, and 10.7% for the SnO_2 nanowire, ZnO nanowire, and In_2O_3 nanowire chemical sensors, respectively. This can be understood, as hydrogen exhibits reducing gas behavior for n-type semiconducting metal oxide nanowires by desorbing absorbed oxygen ions and producing oxygen vacancies [39]. As a result, the nanowire conductance increased with the metal oxide nanowire sensors operated at 200 °C. In contrast, a decrease of 18% in conductance was observed in SWNT chemical sensor operated at 200 °C with the introduction of 500 ppm hydrogen, as shown in figure 3(a). Furthermore, with the SWNT sensor operated at room temperature, we did not observe any significant conductance change even with the introduction of 2000 ppm hydrogen. Some early reported literatures suggested that the sensing response can happen in the interface of nanomaterials and contact electrodes due to the chemisorption instead of physisorption of hydrogen onto the Pt electrodes [40, 41]. However, the interaction between the interface of nanomaterials and contact electrodes are complex and might not clear till now. Thus further studies are required to investigate the sensing mechanism.

Similar to hydrogen, ethanol also works as a reducing gas to n-type semiconducting metal oxide nanowires, which can be easily observed from figure 3(b). The electrical conductance was initially stable; however, upon exposure to 50 ppm ethanol

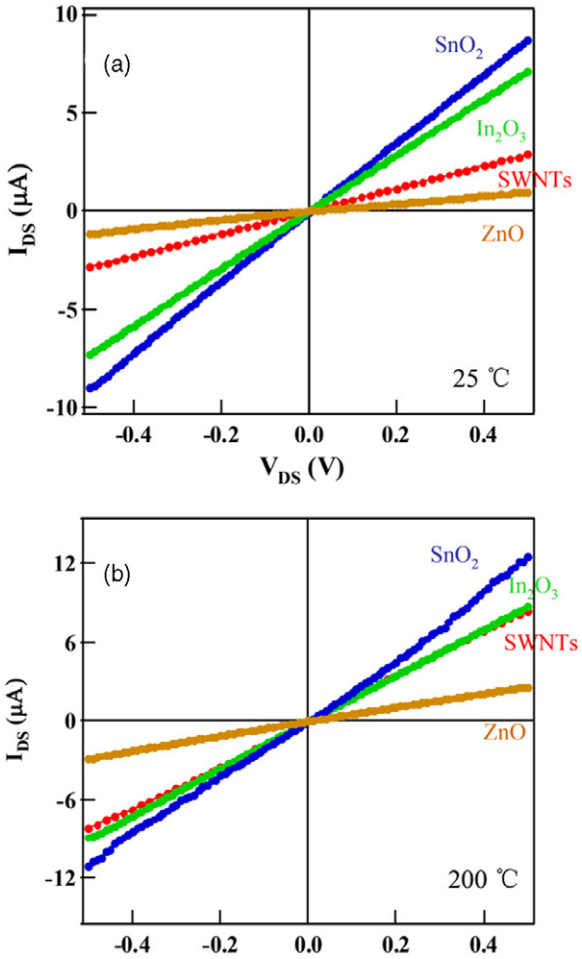

Figure 2. Current–voltage curves of as-fabricated chemical sensors measured at room temperature (a) and 200 °C (b).

diluted in dry air, the conductance was observed to increase by 14.8%, 1.277%, and 16.1% for SnO_2, ZnO, and In_2O_3 nanowire chemical sensors, respectively with the nanosensors kept at 200 °C using the micromachined hot plates. In the meantime, no response was observed with the SWNT chemical sensor even with the introduction of 200 ppm ethanol at 200 °C. As we know, oxygen molecules are usually adsorbed on the surface of various metal oxide nanowires and form negative oxygen ions. These ions lead to a reduction in electron concentration in n-type semiconductors. Once exposed to ethanol vapor at elevated temperatures, these oxygen ions can react with ethanol absorbed on the surface and release electrons back to nanowires. The mechanism is as below [42].

$$C_2H_5OH+O(s)+M(s) \rightarrow C_2H_4O+H-M(ads)+H-O(ads) \quad (2)$$

where (s) and (ads) indicate a surface site or an adsorbed species, respectively.

Previously, several researchers reported the detection of ethanol vapor using multi-walled carbon nanotube (MWNT) thin film sensors at high temperatures and SWNT devices with high gate bias at room temperature in dry nitrogen environment as well [43, 44]. The possible sensing mechanisms in carbon nanotube devices can be attributed to (i) the change of bulk

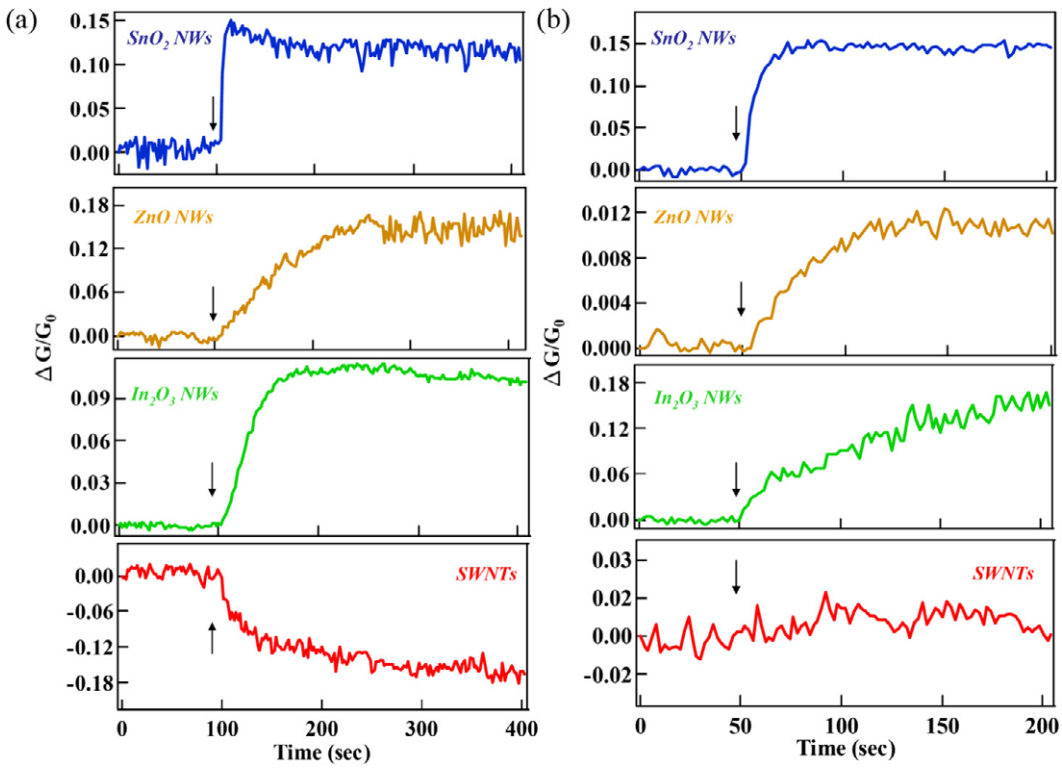

Figure 3. Sensing response to 500 ppm hydrogen (a) and 50 ppm ethanol (b) diluted in air for SnO_2 nanowire, ZnO nanowire, In_2O_3 nanowire, and SWNT sensors operated at 200 °C. The Y-axis represents $\Delta G/G_0$. Arrows indicate time when the tested chemical was flown into the sensing chamber.

doping on nanotube body, (ii) the Schottky barrier induced by gas adsorption at nanotube/metal contact interface, or (iii) the electrochemical reaction of chemical and substrate surface [43, 44]. However, in our case, it is interesting that we did not observe significant change in SWNT nanosensor under exposure of ethanol. In comparison of [44], the observation can be attributed to the different device design, which means that no gate voltage was applied to our SWNT sensors, and the SiN surface we used can be very different from the Si/SiO_2 surface used in [44]. The SWNT sensors, therefore, provide us great discrimination between two different reducing gases, hydrogen and ethanol, with reduced conductance observed for hydrogen exposure, and an absence of conductance change for ethanol exposure.

3.3. Smell-print library

Further measurements using our hybrid nanostructure sensor array were accomplished with different concentrations of hydrogen, ethanol and NO_2 at different temperatures (table 1). Through these sensing measurements, we can go toward a sensor response library of 'smell-print' with the use of this nanosensor array, thus creating an 'electronic nose'. The histogram in figure 4 summarizes the sensing response of these tested gases. The solid bars and shaded bars represent the sensing response at 25 °C and 200 °C, respectively, and the height of each bar indicates the relative sensor response (RS) in conductance which is described as equation (1). As shown in figure 4, SWNT chemical sensors showed significantly different response to each chemical, as compared to In_2O_3, SnO_2, and ZnO nanowire sensors. For example, the RS of the SWNT sensor was about 0.23 at 200 °C and 0.02 at room temperature upon exposure to 0.1 ppm NO_2. A negative response (RS ~ -0.2) at 200 °C and no response (RS ~ 0) at room temperature were observed in the case of H_2 sensing at 500 ppm. Furthermore, there was no observed response (RS ~ 0) to ethanol at room temperature and even at 200 °C for various concentrations. As we discussed in the introduction, the sensing mechanisms between metal oxide nanowire and SWNT sensors are different [35–38]. Thus, metal oxide nanowire sensors usually exhibit opposite sensing response as compared to SWNT sensors upon exposure to the same chemical. Therefore, the SWNT chemical sensor worked as a good 'discrimination factor' for our electronic nose study.

3.4. Principal component analysis

For data analysis, there are several suitable tools, such as independent component analysis (ICA), linear discrimination analysis (LDA), and principal component analysis (PCA) [45]. Among them, both LDA and PCA provide optimal discrimination power [46], but have not been fully explored for nanostructure-based chemical sensor arrays. Generally speaking, LDA is a supervised method (i.e. need calibration of both sensor signals and respective concentrations), which usually requires a relatively large number of samples from each analyte class. PCA, on the other hand, is a powerful unsupervised method (i.e., only require independent variable information

Table 2. Correlation matrix of hybrid sensor array operated at different temperatures.

	SnO_2 (RT)	SnO_2 (HT)	In_2O_3 (RT)	In_2O_3 (HT)	SWNT (RT)	SWNT (HT)	ZnO (RT)	ZnO (HT)
SnO_2 (RT)	1.000	0.976	0.997	0.972	−0.959	−0.933	0.998	0.374
SnO_2 (HT)	—	1.000	0.986	0.996	−0.985	−0.959	0.970	0.421
In_2O_3 (RT)	—	—	1.000	0.982	−0.977	−0.954	0.995	0.383
In_2O_3 (HT)	—	—	—	1.000	−0.981	−0.943	0.966	0.350
SWNT (RT)	—	—	—	—	1.000	0.984	−0.950	−0.400
SWNT (HT)	—	—	—	—	—	1.000	−0.923	−0.517
ZnO (RT)	—	—	—	—	—	—	1.000	0.369
ZnO (HT)	—	—	—	—	—	—	—	1.000

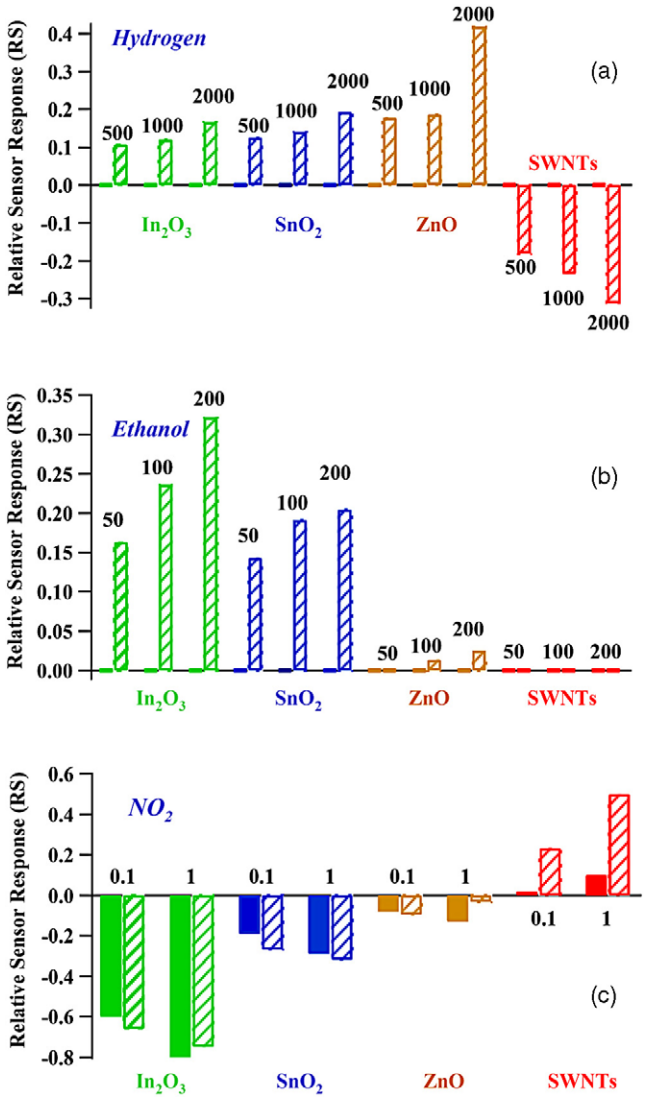

Figure 4. Representative sensor array response as bar graphs to ethanol (a), hydrogen (b), and NO_2 (c). The solid bars and shaded bars represent the sensing response at 25 °C and 200 °C, respectively.

such as sensor responses) and is good for various qualitative applications in understanding relationship in sensing data [46]. It provides an efficient method for reducing the dimensionality of a data set by performing a covariance analysis between various factors [23]. For a data matrix M, with sensing responses from m different samples as row and n sensors as column (in our case, $m = 8$ for eight sensing conditions in table 1, and $n = 8$ for four different sensors operated at two temperatures), the PCA approach carries out singular value decomposition (SVD) [46], which allows projection of the data set in 2D or 3D principal component space. As a result, a correlation between the relative positions of factors and contribution of each sensor in the loading plot (principal component diagram) can be visualized. Thus, PCA not only reveals the redundant information in the data set, but also groups the data with similar characteristics.

To study the discrimination ability of the hybrid sensor array, the PCA analysis was carried out with the aid of commercial statistical software (STATISTIXL 1.7 Beta version). The processed data set contains the sensor responses from 8 sensing components (4 sensors with 2 different operation temperatures) in a sensor array to different chemicals with different concentrations. Figure 5(a) shows the score and loading plots of the first two principal components (PC1 and PC2) for the data of the metal oxide nanowire and SWNT sensor array responses to the tested chemicals, hydrogen, ethanol, and NO_2, respectively. The cumulative variance of PC1 and PC2 is 98.1%, which is considered to be good in retaining the originality of the data [23]. These chemicals were clearly separated to 3 clusters in principal component space, which indicates that this sensor array provides a high discrimination ability in respect to these chemicals. Comparing to conventional chemical sensing results and sensors, the hybrid sensor array developed in this work can distinguish chemicals by their nature rather than their concentrations. In addition, we have found that the integration of carbon nanotube sensors played an important role in improving the selectivity of the electronic nose system.

Figure 5(b) displays the PCA plot based on sensing results from only the In_2O_3, SnO_2, and ZnO nanowires. Although NO_2, hydrogen and ethanol can still be distinguished to certain degree, there is a slight overlap between ethanol and hydrogen clusters. By comparing figures 5(a) and (b), one can clearly see the importance of integrating both metal oxide nanowires and carbon nanotubes for the maximized discrimination power of electronic noses. Table 2 shows the correlation matrix of hybrid sensor array operated at different temperatures. As one can see, the strong correlation is found among most of metal oxide nanowire sensors operated at both high and room temperatures. Only ZnO nanowire sensor operated at 200 °C appears to be moderately independent from other metal oxide nanowire sensors. Besides, SWNT sensors also show a strong correlation at both high and room operation

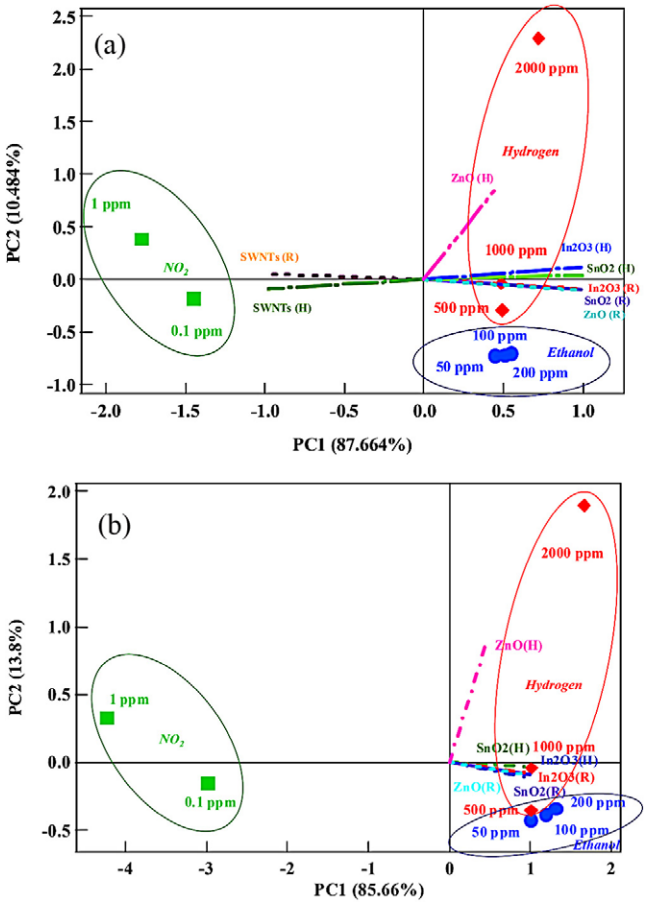

Figure 5. PCA scores and loading plots of the chemical sensor array composed by 4 different nanostructure materials (a) and only 3 metal oxide nanowires (b) operated at different concentrations and temperatures.

temperatures to each other. This probably can be attributed to that individual sensors in a sensor array have poor specificity in chemicals [23]. Further experiments/modeling are needed to investigate this observation. Besides, in order to identify and quantify the test chemicals, other classification techniques (ex. LDA and artificial neural networks) need to be applied in future works.

4. Conclusion

In summary, we demonstrated a brand-new hybrid chemical sensor array composed of In_2O_3 nanowire, SnO_2 nanowire, ZnO nanowire, and SWNT sensors, which were integrated with micromachined hot plates. Key to our success includes the integration of nanowire and carbon nanotube sensors, precise control of the sensor temperature, and the use of principal component analysis for data processing. The response of these sensors to hydrogen, ethanol, and NO_2 were measured at different concentrations and at both room temperature and 200 °C. Principal component analysis of the sensing results showed great discrimination of those three tested chemicals, and in-depth analysis revealed clear improvement of selectivity by the integration of carbon nanotube sensors. This nanoelectronic nose approach has great potential to detect and discriminate a wide variety of gases, including explosives and nerve agents.

Acknowledgments

We acknowledge financial support from the National Science Foundation (CCF 0726815 and CCF 0702204).

References

[1] Cui Y, Wei Q, Park H K and Lieber C M 2001 *Science* **293** 1289
[2] Maiti A, Rodriguez J A, Law M, Kung P, McKinney J R and Yang P 2003 *Nano Lett.* **3** 1025
[3] Kong J, Franklin N R, Zhou C, Chapine M G, Peng S, Cho K and Dai H 2000 *Science* **287** 622
[4] Yu C, Han Q, Saha S, Shi L, Kong X and Wang Z L 2005 *Appl. Phys. Lett.* **86** 063101
[5] Zhang D, Liu Z, Li C, Tang T, Liu X, Han S, Lei B and Zhou C 2004 *Nano Lett.* **4** 1919
[6] Staii C, Johnson A T Jr, Chen M and Gelperin A 2005 *Nano Lett.* **5** 1774
[7] Lao C, Li Y, Wong C P and Wang Z L 2007 *Nano Lett.* **7** 1323
[8] Qi P, Vermesh O, Grecu M, Javey A, Wang Q and Dai H 2003 *Nano Lett.* **3** 347
[9] Lu Y, Partridge C, Meyyappan M and Li J 2006 *J. Electroanal. Chem.* **593** 105
[10] Star A, Joshi V, Skarupo S, Thomas D and Gabriei J-C P 2006 *J. Phys. Chem.* B **110** 21014
[11] Tien L C, Sadik P W, Norton D P, Voss L F, Pearton S J, Wang H T, Kang B S, Ren F, Jun J and Lin J 2005 *J. Appl. Phys. Lett.* **87** 222106
[12] Sysoev V V, Button B K, Wepsiec K, Dmitriev S and Kolmakov A 2006 *Nano Lett.* **6** 1584
[13] Chen X H and Moskovits M 2007 *Nano Lett.* **7** 807
[14] Kolmakov A, Klenov D O, Lilach Y, Stemmer S and Moskovits M 2005 *Nano Lett.* **5** 667
[15] McApline M C, Ahmad H, Wang D and Heath J R 2007 *Nat. Mater.* **6** 379
[16] Snow E S, Perkins F K, Houser E J, Badescu S C and Reinecke T L 2005 *Science* **307** 1942
[17] Fan Z Y and Lu J G 2005 *Appl. Phys. Lett.* **86** 123510
[18] *DE Patent Specification* 4423289
EP Patent Specification 0769141B
US Patent Specification 5783154
JP Patent Specification 2980688C
[19] Goschnick J, Haeringer D and Kiselev I 2007 *Sensors Actuators* B **127** 237
[20] Sysoev V V, Goschnick J, Schneider T, Strelcov E and Kolmakov A 2007 *Nano Lett.* **7** 3182
[21] Arnold C, Harms M and Goschnick J 2002 *IEEE Sensors J.* **2** 179
[22] Ryu K, Zhang D and Zhou C 2008 *Appl. Phys. Lett.* **9** 093111
[23] Srivastave A K and Dravid V P 2006 *Sensors Actuators* B **117** 244
[24] Scorsone E, Pisanelli A M and Persaud K C 2006 *Sensors Actuators* B **116** 55
[25] Scott S M, James D and Ali Z 2007 *Microchim. Acta* **156** 183
[26] Li C, Zhang D, Han S, Liu X, Tang T and Zhou C 2003 *Adv. Mater.* **15** 143
[27] Liu Z, Zhang D, Han S, Li C, Tang T, Jin W, Liu X, Lei B and Zhou C 2003 *Adv. Mater.* **15** 1754
[28] Xiang B, Wang P, Zhang X, Dayeh S A, Aplin D P R, Soci C, Yu D and Wang D 2007 *Nano Lett.* **7** 323
[29] Han S, Zhang D and Zhou C 2006 *Appl. Phys. Lett.* **88** 133109

[30] Liu X, Lee C, Han S, Li C and Zhou C 2003 *Molecular Nanoelectronics* (New York, USA: American Scientific Publishers) p 2
[31] Li C, Lei B, Zhang D, Liu X, Han S, Tang T, Rouhanizadeh M, Hsiai T and Zhou C 2003 *Appl. Phys. Lett.* **83** 4014
[32] Li C, Zhang D, Liu X, Han S, Tang T, Han J and Zhou C 2003 *Appl. Phys. Lett.* **82** 1613
[33] Li C, Zhang D, Han S, Liu X and Zhou C 2003 *J. Phys. Chem.* B **107** 12451
[34] Zhang D, Li C, Liu X, Han S, Tang T and Zhou C 2003 *Appl. Phys. Lett.* **83** 1845
[35] Chen P C, Shen G and Zhou C 2008 *IEEE Trans. Nanotechnol.* **7** 668
[36] Barsan N and Weimar U 2001 *J. Electroceram.* **7** 143
[37] Batzill M and Diebold U 2005 *Prog. Surf. Sci.* **79** 47
[38] Zhao J J, Buldum A, Han J and Lu J 2002 *Nanotechnology* **13** 195
[39] Fryberger T B and Semancik S 1990 *Sensors Actuators* B **2** 305
[40] Dag S, Ozturik Y, Ciraci S and Yildirim T 2005 *Phys. Rev.* B **72** 155404
[41] Kumar M K and Ramaprabhu S 2006 *J. Phys. Chem.* B **110** 11291
[42] Comini E, Faglia G, Sberveglieri G, Calestani D, Zanotti L and Zha M 2005 *Sensors Actuators* B **111/112** 2
[43] Sin M L Y, Chow G C T, Wong G M K, Li W J and Leong P H W 2007 *IEEE Trans. Nanotechnol.* **6** 571
[44] Someya T, Small J, Kim P, Nuckolls C and Yardley J T 2003 *Nano Lett.* **3** 877
[45] Delac K, Grgic M and Grgic S 2005 *Int. J. Imaging Syst. Technol.* **15** 252
[46] Jurs P C, Bakken G A and McClelland H E 2000 *Chem. Rev.* **100** 2649